Direct observation of R-loop formation by single RNA-guided Cas9 and Cascade effector complexes

Mark D. Szczelkun[a,1,2], Maria S. Tikhomirova[b,c,1], Tomas Sinkunas[d], Giedrius Gasiunas[d], Tautvydas Karvelis[d], Patrizia Pschera[c], Virginijus Siksnys[d,2], and Ralf Seidel[b,c,2]

[a]DNA-Protein Interactions Unit, School of Biochemistry, University of Bristol, Bristol BS8 1TD, United Kingdom; [b]Institute for Molecular Cell Biology, Westfälische Wilhelms-Universität Münster, 48149 Münster, Germany; [c]Biotechnology Center, Technische Universität Dresden, 01062 Dresden, Germany; and [d]Department of Protein–Nucleic Acid Interactions, Institute of Biotechnology, Vilnius University, LT-02241 Vilnius, Lithuania

Edited by Stephen C. Kowalczykowski, University of California, Davis, CA, and approved May 1, 2014 (received for review February 10, 2014)

Clustered, regularly interspaced, short palindromic repeats (CRISPR)/CRISPR-associated (Cas) systems protect bacteria and archaea from infection by viruses and plasmids. Central to this defense is a ribonucleoprotein complex that produces RNA-guided cleavage of foreign nucleic acids. In DNA-targeting CRISPR-Cas systems, the RNA component of the complex encodes target recognition by forming a site-specific hybrid (R-loop) with its complement (protospacer) on an invading DNA while displacing the noncomplementary strand. Subsequently, the R-loop structure triggers DNA degradation. Although these reactions have been reconstituted, the exact mechanism of R-loop formation has not been fully resolved. Here, we use single-molecule DNA supercoiling to directly observe and quantify the dynamics of torque-dependent R-loop formation and dissociation for both Cascade- and Cas9-based CRISPR-Cas systems. We find that the protospacer adjacent motif (PAM) affects primarily the R-loop association rates, whereas protospacer elements distal to the PAM affect primarily R-loop stability. Furthermore, Cascade has higher torque stability than Cas9 by using a conformational locking step. Our data provide direct evidence for directional R-loop formation, starting from PAM recognition and expanding toward the distal protospacer end. Moreover, we introduce DNA supercoiling as a quantitative tool to explore the sequence requirements and promiscuities of orthogonal CRISPR-Cas systems in rapidly emerging gene-targeting applications.

magnetic tweezers | genome engineering | crRNA

Clustered, regularly interspaced, short palindromic repeats (CRISPR)/CRISPR-associated (Cas) systems constitute an adaptable immune system that protects bacteria and archaea against foreign nucleic acids. The defense is initiated by a ribonucleoprotein (RNP) complex that mediates cleavage of dsDNA (1) or RNA (2, 3). The RNA component (crRNA) of the complex is derived by transcription and posttranscriptional processing from a locus containing CRISPRs (2, 4, 5) in which short spacer fragments were integrated from foreign nucleic acids (6–8). Each transcribed crRNA spacer sequence encodes the recognition of the targets. In DNA-targeting CRISPR-Cas systems, the crRNAs form a hybrid with a matching complement (protospacer) on an invading DNA, which leads to the displacement of the noncomplementary strand. The resulting structure is called an R-loop and constitutes the signal for subsequent DNA degradation. R-loop formation is additionally dependent on a short protospacer adjacent motif (PAM) (Fig. 1*A*), which provides discrimination between self and nonself DNA in CRISPR systems; it is absolutely required for recognition of the invading DNA but is absent from the host CRISPR array (9).

On the basis of sequence homology, different CRISPR-Cas families have been identified (10). We investigate here a type IE and a type II system from *Streptococcus thermophilus St*-CRISPR4 and *St*-CRISPR3, respectively. The Cas proteins of type IE systems (4, 11, 12) associate with a crRNA into a multisubunit ~400-kDa RNP ($CasA_1B_2C_6D_1E_1$) called "Cascade" (4, 12). The crRNA is anchored at its 5′-hydroxyl and 2′,3′-cyclic phosphate termini, respectively, by CasA and CasE, which are bridged by a helical $CasC_6$ nucleoprotein filament (13). In the type IE *St*-CRISPR4 system, complementary binding of the crRNA to the protospacer should generate an R-loop of 33 nt (Fig. 1*A*). Target DNA degradation is accomplished by the helicase–nuclease Cas3 recruited to the R-loop (12, 14, 15). The PAM in *St*-CRISPR4 is relatively promiscuous: a dinucleotide AA supports optimal cleavage, whereas CC suppresses activity. For type II systems, the RNP complex comprises only a single-subunit ~180-kDa Cas9 protein bound to a dual crRNA-tracrRNA (16–18). The Cas9 RNP executes both R-loop formation and DNA cleavage. In the type II *St*-CRISPR3 system, the PAM sequence is GGNG (16), and complementary binding with only part of the protospacer sequence results in a putative 20-nt R-loop (Fig. 1*A*).

R-loop formation and full DNA degradation reactions by CRISPR-Cas systems have been previously reconstituted (12, 14, 16, 17). For the R-loop formation process, in which the DNA duplex is unwound without external energy, a unidirectional model has been proposed (19, 20). After PAM recognition by the RNP, priming of the R-loop adjacent to the PAM would lead to unidirectional expansion toward the distal protospacer end. The model was supported by observations that a mutated PAM or mismatches between crRNA and protospacer adjacent to the PAM have more severe effects on DNA cleavage than distal mismatches (19, 20) and, as recently reported, on the time Cas9 spends on the target (21). This assumes that mutations within or adjacent to the PAM impede R-loop formation. An alternative explanation would be that R-loops still form with significant

Significance

Clustered, regularly interspaced, short palindromic repeats (CRISPR)/CRISPR-associated (Cas) systems provide adaptive immunity for bacteria and archaea. They use a protein complex that targets invading nucleic acids using a bound RNA that hybridizes to complementary sequence stretches. On DNA targets, the resulting structure is an R-loop. By twisting single DNA molecules, we can directly observe R-loop formation and dissociation in two distinct types of CRISPR-Cas system. This allows us to investigate the role of different elements of the target sequence. Whereas upstream elements control the actual R-loop formation, downstream elements ensure R-loop stability, suggesting a directional R-loop formation. This provides insight into the recognition process by these enzymes, which is the crucial step to understand targeting in the rapidly emerging genetic engineering applications of CRISPR-Cas systems.

Author contributions: M.D.S., V.S., and R.S. designed research; M.D.S., M.S.T., T.S., G.G., T.K., P.P., and R.S. performed research; M.D.S., M.S.T., T.S., G.G., T.K., P.P., V.S., and R.S. analyzed data; and M.D.S., V.S., and R.S. wrote the paper.

The authors declare no conflict of interest.

This article is a PNAS Direct Submission.

[1]M.D.S. and M.S.T. contributed equally to this work.

[2]To whom correspondence may be addressed. E-mail: mark.szczelkun@bristol.ac.uk, siksnys@ibt.lt, or ralf.seidel@uni-muenster.de.

This article contains supporting information online at www.pnas.org/lookup/suppl/doi:10.1073/pnas.1402597111/-/DCSupplemental.

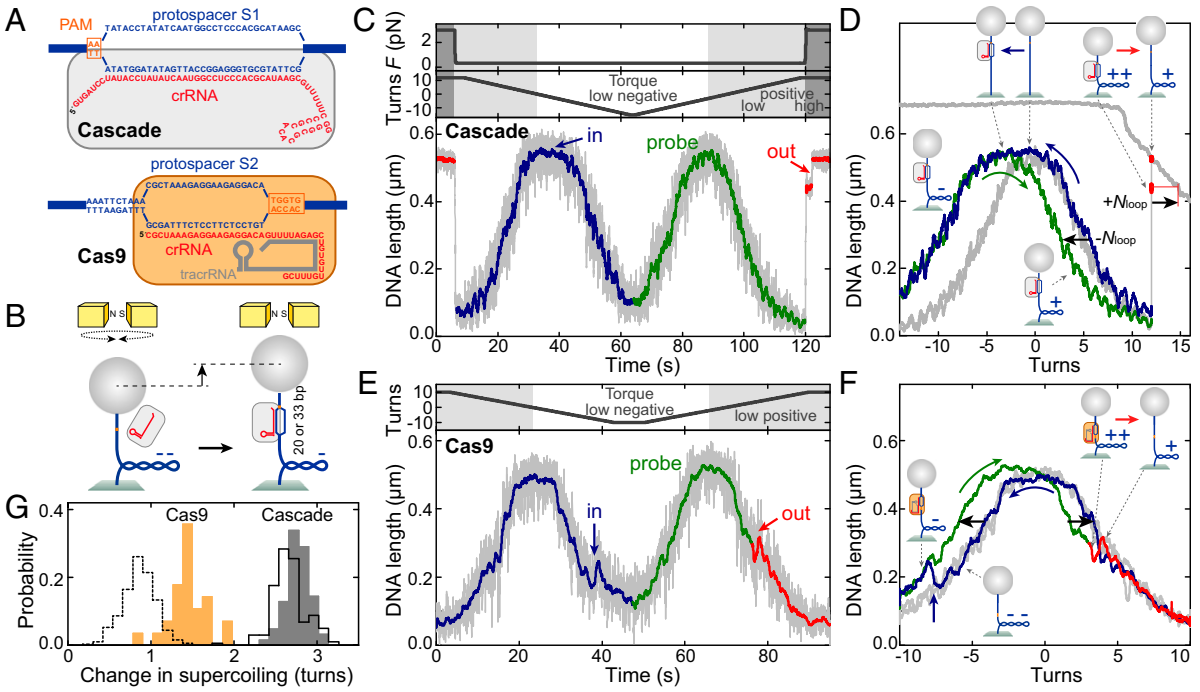

Fig. 1. R-loop formation and dissociation by Cascade and Cas9 observed in single-molecule twisting experiments. (*A*) Schematics of the anticipated R-loops formed by Cascade (33 bp) and Cas9 (20 bp). (*B*) Magnetic tweezers-based twisting assay. R-loop formation on supercoiled DNA molecules at fixed rotation causes local DNA untwisting. Compensatory overtwisting of the DNA changes the supercoiling, resulting in a DNA length change (see also *SI Appendix*, Fig. S1*A*). (*C* and *D*) R-loop cycle experiment in the presence of 10 nM Cascade. DNA with matching protospacer/PAM (*A*) is negatively supercoiled at 0.31 pN to induce R-loop formation (blue area of trace), followed by positive supercoiling to probe: the presence of the R-loop (green area of trace); and R-loop dissociation at an increased force of 3.0 pN (red area of trace). Blue and red arrows indicate the positions of R-loop formation and dissociation, respectively. In *D*, the lower and upper gray supercoiling curves were taken on the same DNA molecule at 0.31 and 3.0 pN, respectively, before Cascade addition. (*E* and *F*) R-loop cycle experiment in the presence of 1 nM Cas9 on DNA containing a matching protospacer/PAM (*A*) at a constant force of 0.31 pN. R-loop dissociation occurs readily at low positive torque. (*G*) Cas9-induced shift of the supercoiling curve (orange bars). For Cascade, shifts of the right part of the supercoiling curve after R-loop formation (gray bars; $-N_{loop}$ in *D*) and after full R-loop dissociation (bars with solid black outline; $+N_{loop}$ in *D*; also see *SI Appendix, SI Methods*) are shown. Bars with dashed black outline show the shift of the first R-loop dissociation substep for Cascade (Fig. 2*A*).

efficiency but display a reduced lifetime, the magnitude of which depends on the position of the mutation. These alternatives represent target/PAM verification by either kinetic inhibition or altered equilibrium.

To clearly distinguish between the two models, we use here single-molecule DNA supercoiling to directly reveal the kinetics and the extent of R-loop formation and dissociation (22–24). Moreover, our assay provides quantitative insight into the dependence of these processes on DNA supercoiling. For both CRISPR-Cas systems investigated, the PAM is found to affect exclusively the R-loop association rates. Nonetheless, R-loops with unaltered stability can even form for PAM mutants that do not support cleavage. Conversely, protospacer elements distal to the PAM affect primarily R-loop stability but not R-loop formation rates. This provides direct evidence for the unidirectional R-loop formation model and a target/PAM verification by kinetic inhibition. Additionally, our data reveal important differences between the Cascade and the Cas9 based CRISPR-Cas systems.

Results and Discussion

Direct Observation of R-Loop Formation in Real Time. To observe R-loops in single DNA molecule supercoiling experiments, we used magnetic tweezers (23, 25) (Fig. 1*B*). A 2.1-kbp DNA containing a single protospacer and PAM was attached at one end to a magnetic bead and at the other end to the bottom of a fluidic cell. A pair of magnets above the cell was used to stretch the DNA and to supercoil it by rotating the magnets. Simultaneously the DNA length was measured (26). Upon supercoiling DNA at constant force, its length stays initially constant. Once a critical torque in the molecule is reached, its length starts to decrease because of formation of a plectonemic superhelix resulting in a characteristic rotation curve and an associated torque profile (Fig. 1*B* and *SI Appendix*, Fig. S1) (25, 27–29). Enzyme-dependent local DNA unwinding (e.g., attributable to R-loop formation) changes the DNA twist and can be seen as a shift of the whole rotation curve or as a DNA length change (22) (Fig. 1*B* and *SI Appendix*, Fig. S1). To detect R-loop formation, we carried out "R-loop cycles" with Cascade or Cas9 on DNA with matching protospacer and canonical PAM sequences (Fig. 1*A*). First, we slightly untwisted the DNA (producing negative supercoiling) at low force to help R-loop formation (blue curves in Fig. 1 *C*–*F*). Subsequently, we probed R-loop dissociation by rewinding the DNA to produce positive supercoiling (green curves in Fig. 1 *C*–*F*). For both enzymes, we observed efficient R-loop formation (100% of all cases; $n = 89$ and 50, respectively), which was seen as a shift of the left side of the probe curve toward negative turns compared with the curve in absence of the proteins (Fig. 1 *D* and *F*). Whereas Cascade formed an R-loop instantaneously at low negative supercoiling (−1 to −2 turns), Cas9 required longer times and more negative supercoiling. For Cascade, the R-loop was stable at positive turns and low force, seen as a stable shift of the right side of the probe curve (Fig. 1*D*). R-loop dissociation could be observed at elevated force (corresponding to elevated positive torque) as an abrupt length jump (Fig. 1 *C* and *D*). In contrast, Cas9-induced R-loops dissociated readily at low positive force (Fig. 1 *E* and *F*). The observed shifts in the rotation curves were dependent on the presence of a protein complex, a matching protospacer, and a corresponding crRNA (*SI Appendix*, Fig. S2). For Cascade, the right part of the supercoiling curve shifted by −2.62 ± 0.04 turns

(formation) and +2.67 ± 0.03 (dissociation), whereas the center of the curve moved by 2.81 ± 0.07 turns (Fig. 1*G* and *SI Appendix*, Fig. S3). For Cas9, 1.45 ± 0.05 turns were obtained from the center shift (Fig. 1*G*). These values are slightly smaller than anticipated (3.1 and 1.9 turns considering a DNA helical pitch of 10.5 bp), possibly because of compensatory writhe from DNA bending induced by effector binding (14).

Torque Dependence of R-Loop Formation and Dissociation. To obtain insight into the previously proposed regulation of R-loop formation by supercoiling (14) and into the energetics of the R-loop structure, we quantified the R-loop formation and dissociation kinetics as a function of the applied torque (see *SI Appendix*, *SI Theory* for torque determination) from repeated R-loop cycles (Fig. 2 *A* and *D*). For Cascade, both R-loop formation and dissociation were torque-dependent (Fig. 2*B* and *SI Appendix*, Fig. S4). R-loop dissociation required an ∼fourfold higher absolute torque value than formation. Most dissociation events (76%; n = 482) displayed a short-lived and torque-dependent intermediate state corresponding to 0.9 ± 0.1 turns (Figs. 1*G* and 2 *A* and *B*). By fitting the torque dependence of the kinetics to an Arrhenius-like model (Fig. 2*B*; also see *SI Appendix*, *SI Theory*), we could calculate the transition state distances (ΔN_{in} = 1.5 ± 0.2 turns for R-loop formation; ΔN_{out}^{1} = 0.31 ± 0.5 and ΔN_{out}^{2} = 0.15 ± 0.06 turns for the two dissociation intermediates). From the mean transition times in the absence of torque, a free energy gain for R-loop formation of 2.1–6.3 k_BT was determined (*SI Appendix*, *SI Theory*). A simplified energy landscape for R-loop formation by Cascade is suggested (Fig. 2*C*), using the transition state distances combined with the rotational shifts for full and intermediate R-loop states. For Cas9, R-loop dissociation occurred in a single measurable and torque-dependent step at ∼fivefold lower torque compared with Cascade, with ΔN_{out} = 0.5 ± 0.1 (Fig. 2 *D* and *E* and *SI Appendix*, Fig. S4). Whereas R-loop dissociation was independent of Cas9 concentration as expected, R-loop formation was limited by Cas9 binding to the target site (see Cas9 concentration dependence in Fig. 2*E*), such that any torque dependence was masked. Therefore, an energy landscape for Cas9 cannot yet be determined.

PAM Mutations Hinder R-Loop Formation but Not Its Stability in Both Systems. To clarify whether the PAM regulates R-loop formation by kinetic inhibition or altered R-loop stability, we measured the dynamics of R-loop formation and dissociation on substrates with matching protospacers but mutated PAMs. For Cascade, we compared four PAMs with affinities following the order AA > TT > AG >> CC (12). The TT and AG PAMs still support Cas3-dependent DNA degradation, which is completely abolished for the CC dinucleotide (12). Although we observed efficient R-loop formation for the TT and AG PAMs, higher negative turns/torque were required compared with the AA PAM (Fig. 3 *A* and *B*). In contrast, the torque-dependent mean dissociation times of both substeps were unchanged within error, suggesting that the R-loops are equally stable once formed. Following the same protocol using the CC PAM, we were unable to observe any R-loops. However, R-loops could be induced with moderate efficiencies at elevated forces and high negative twist [35% of all attempts for −200 turns (n = 51); 19% for −100 turns (n = 27); 0% at −10 turns (n = 78)], conditions that mechanically cause extensive DNA denaturation. R-loops for the CC PAM were also

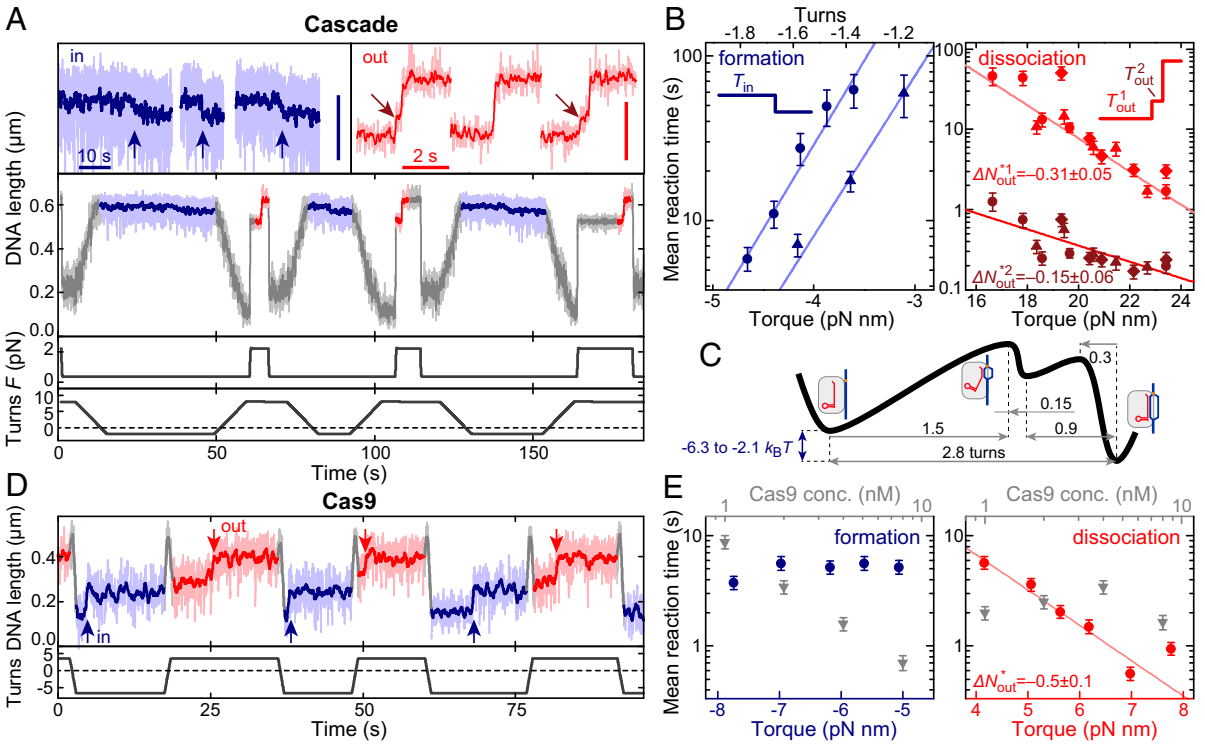

Fig. 2. Torque dependence of R-loop formation and dissociation by Cascade and Cas9. (*A*) Repetitive cycles of R-loop formation (at −1.6 turn, 0.36 pN) and R-loop dissociation (at +8 turns, 2.2 pN) by Cascade. R-loop formation and dissociation is seen as a DNA length decrease or increase, respectively (enlarged views on top). (Vertical scale bars: 100 nm.) Blue arrows indicate R-loop formation, and brown arrows indicate a short-lived intermediate state upon R-loop dissociation. (*B*) Mean R-loop formation times (blue scatter plots) and dissociation times (red and brown scatter plots for the first and second dissociation step, respectively) as a function of torque. Different symbols indicate measurements on different DNAs to show experimental variation. Solid lines are exponential fits to the data according to *SI Appendix*, Eqs. **S8** and **S9**. Numbers indicate distances to the transitions states as obtained from the fits. (*C*) Energy landscape of the R-loop formation process by Cascade based on the torque dependency. (*D*) Repetitive cycles of R-loop formation (at −6 turns; blue stretches) and R-loop dissociation (at +3 turns; red stretches) by Cas9. A constant force of 0.31 pN was applied. Red arrows indicate dissociation events. (*E*) Mean R-loop formation and dissociation times as a function of torque (at 1 nM Cas9) and of Cas9 concentration (at a torque of −6.2 and +6.2 pN nm).

stable. While the torque-dependent mean time for the first dissociation step of the CC DNA was indistinguishable from the other PAMs, the mean time for the second step was significantly reduced (Fig. 3*B*). Compared with Cascade, PAM recognition for Cas9 appeared to be more stringent. R-loops could still be formed using a G4C mutant, albeit at a much lower rate (Fig. 3*C*). Once formed, R-loop stability was not compromised (Fig. 3*D*). R-loop formation using G1C and G2C was even slower, whereas PAM deletion did not support R-loop formation at all, even under induced denaturation conditions (*SI Appendix*, Fig. S5). In support of the tweezer data, DNA cleavage assays suggest that R-loop formation is hindered by PAM mutation (with the order G2C > G1C > G4C >> WT) but that subsequent R-loop cleavage is much less affected (*SI Appendix*, Fig. S6). Thus, for both systems, the PAM regulates R-loop formation and subsequent cleavage by kinetic inhibition.

DNA-Helix Destabilization by Cascade. To further explore the role of the PAM during target site search and priming of the R-loop, we carried out supercoiling experiments on DNA without a matching protospacer (but with multiple orphan PAMs; *SI Appendix*, Fig. S7). Interaction with PAMs may result in changes in DNA structure as the CRISPR enzymes probe the adjacent protospacer for complementarity. In line with this, Cascade globally destabilized the DNA helical structure, an effect that required the bound CasA subunit (*SI Appendix*, Fig. S8). The observed behavior agrees only with DNA destabilization (i.e., lowering of the melting temperature) but not with active DNA helix distortion, as seen for DNA intercalators, where stable supercoiling changes are observed (30, 31). Insertion of aromatic amino acid residues of the CasA subunit into the DNA helix (32) may be responsible for the helix destabilization but will be a transient rather than a stably bound state. The destabilization may also cause the PAM dependence of the second dissociation step for Cascade (Fig. 3*B*). Helix-destabilization activity was not found using Cas9.

Protospacer End Truncations Alter R-Loop Stability and Reveal a Conformational Lock for Cascade. For both proteins, the PAM seems to exclusively control R-loop formation, while not affecting R-loop stability once formed. To further test a unidirectional R-loop formation mechanism, we determined the effect of protospacer truncations at the end opposite from the PAM on the dynamics of R-loop formation (Fig. 4 *A* and *C*). For Cascade, R-loops formed efficiently at low negative twist on all substrates truncated by up to 10 bp (as seen by the shift of the left side of the supercoiling curve; Fig. 4*A*). The size of the shifts decreased with increasing truncation, in line with a decrease in R-loop size correlated with complementarity (Fig. 4*A*). For truncations of 6 bp and above, R-loops were formed but were unstable and dissociated as soon as low positive turns at low force were reached; thus, dissociation rates could not be measured (Fig. 4*A* and *SI Appendix*, Fig. S9*A*). For truncations of 2 and 4 bp, both stable and unstable R-loops were observed (Fig. 4*A*). By increasing the experimental waiting time at negative twist during R-loop induction for the 4-bp truncation, the proportion of stable R-loops increased when subsequently probed (*SI Appendix*, Fig. S9*B*), suggesting that stable R-loops originate from an unstable R-loop intermediate. The transition from the unstable to stable R-loop thus locks the R-loop, so that it resists higher torsion compared with Cas9. For the stable R-loops, the stability relative to the full protospacer was only minimally reduced for the 2-bp truncation but was more significantly reduced for the 4-bp truncation, in particular for the first dissociation step (Fig. 4*B*). DNA degradation experiments furthermore revealed that a locked-and-stable R-loop is the prerequisite for Cas3 recruitment and subsequent DNA degradation (*SI Appendix*, Fig. S9*C*).

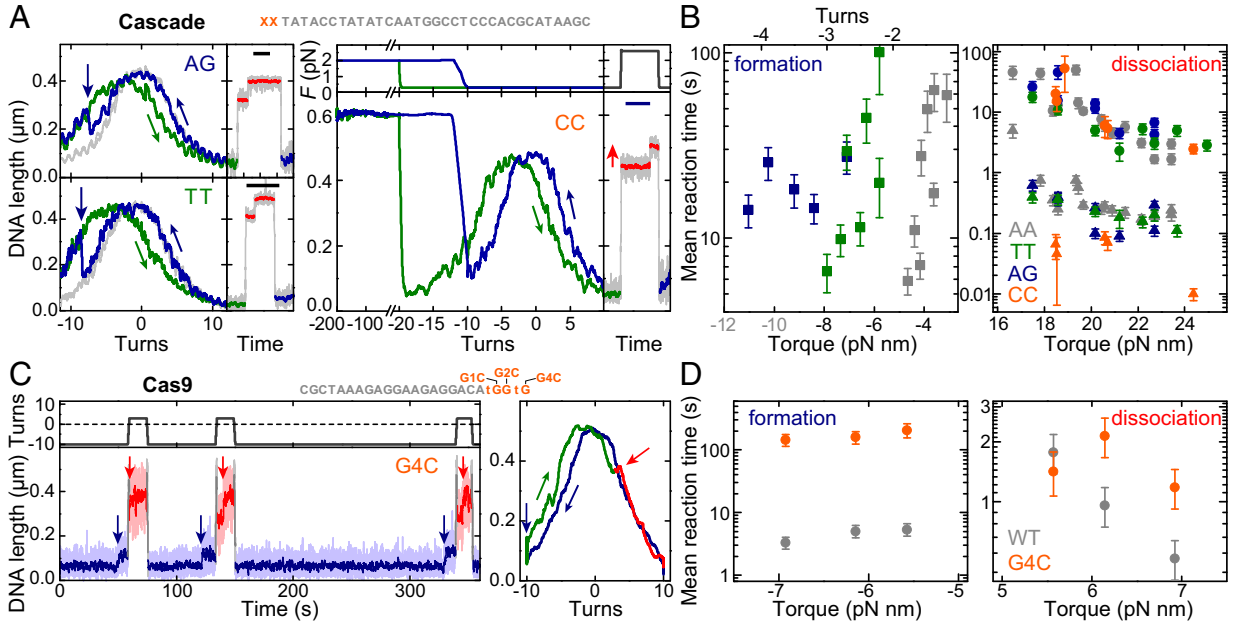

Fig. 3. PAM mutations affect primarily R-loop formation and not dissociation. (*A*) Repetitive R-loop cycles in the presence of Cascade on DNA with the matching protospacer S1 but modified dinucleotide PAMs (see sketch above and labels in the graphs). Curve coloring and experimental conditions are as in Fig. 1 *C* and *D*. For the CC PAM, R-loop formation requires −200 turns (at 2.0 pN; blue curve). The shift in the probe curve (green) and the dissociation step (red curve) reveals the presence of the R-loop. (Scale bars: 10 s.) (*B*) Mean R-loop formation and dissociation times as a function of torque for the different PAMs (colors given in the key). Circles and triangles indicate the first and second dissociation step, respectively. Gray torque values indicate the phase where the torque is no longer proportional to turns. (*C*) Repetitive cycles of R-loop formation and dissociation by Cas9 (as in Fig. 2*D*) at 0.31 pN using a DNA with protospacer S2 and G4C PAM (see sketch). (*D*) Mean R-loop formation and dissociation times as a function of torque for the G4C PAM compared with the canonical PAM.

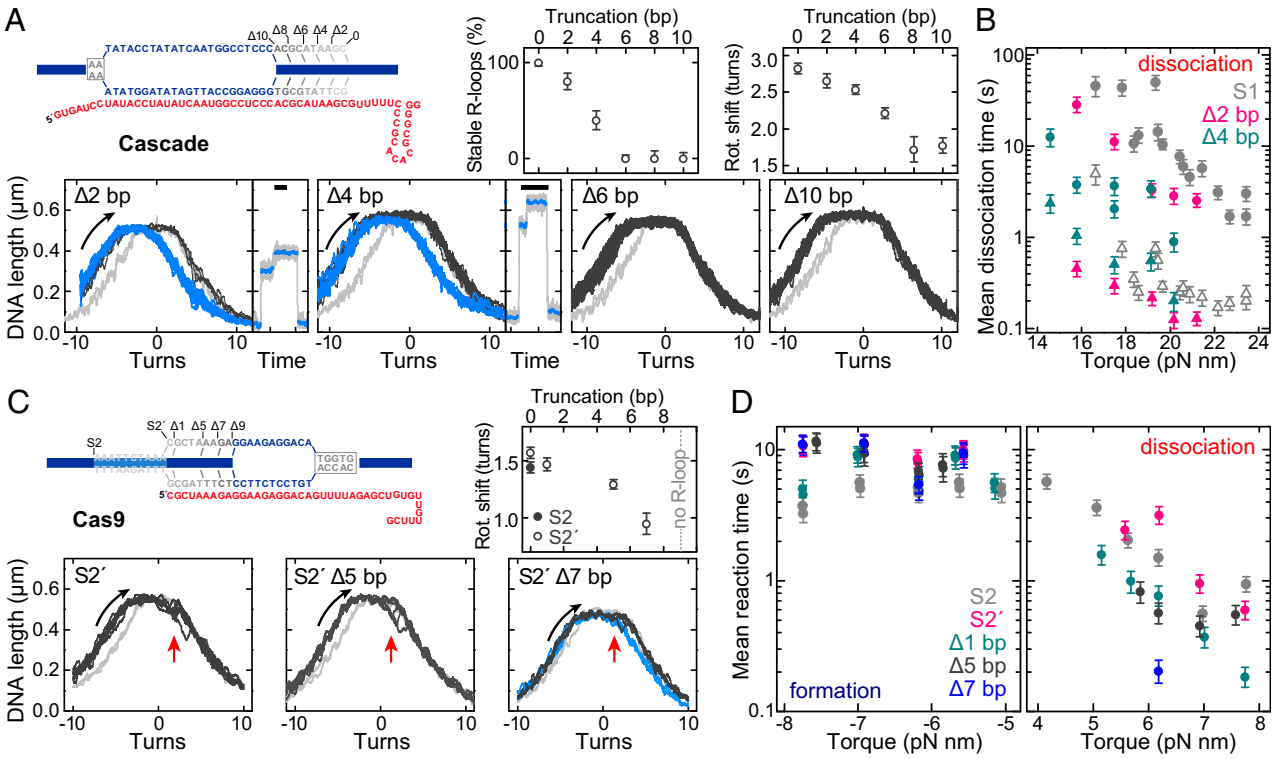

Fig. 4. Protospacer end truncations affect the R-loop stability and reveal a locking mechanism for Cascade but not for Cas9. (*A*) R-loop probe and dissociation curves in the presence of Cascade for protospacer S1 truncated by 2, 4, 6, and 10 bp (see sketch above), revealing stable R-loops (blue) and unstable R-loops (dark gray). Percentages of stable R-loops and the sizes of the rotational shifts are shown in the upper graphs. (*B*) Mean dissociation times as function of torque (from experiments in *A*) for the stable R-loops of 0-, 2-, and 4-bp truncations. Filled circles and open triangles indicate the first and second dissociation step, respectively. (*C*) R-loop probe curves in the presence of Cas9 for protospacer S2′ and truncations of S2′ by 5 and 7 bp (see sketch) revealing R-loops with fast dissociation kinetics (dark gray; red arrows indicate dissociation event) and, in the case of Δ7 bp, additional slow dissociation kinetics (blue). Light gray curves were taken in absence of Cascade or Cas9. The sizes of the rotational shifts are shown in the upper graph. (*D*) Mean formation and dissociation times as a function of torque (from experiments in *C*) for different S2′ protospacer truncations.

Protospacer End Truncations Destabilize R-Loops for Cas9. For Cas9, R-loops were detected for truncations up to 7 bp with little change in the association rate (Fig. 4*C*) but were not detected for a 9-bp truncation (*SI Appendix*, Fig. S10). As above, the size of the rotational shifts correlated with changes in R-loop size (Fig. 4*C*). For 1- or 5-bp truncations, R-loop stability and DNA cleavage rates were slightly reduced (Fig. 4 and *SI Appendix*, Figs. S6 and S10). For the 7-bp truncation, however, although an R-loop population with reduced stability was also detected (Fig. 4*D*), many R-loops exhibited slower, torque-independent dissociation kinetics (*SI Appendix*, Fig. S10). This suggests that mismatches between the crRNA and protospacer can cause rearrangement of the Cas9 RNP into an inhibited, off-pathway intermediate; the protospacer truncation correlated with changes in DNA cleavage rate but also with an accumulation of nicked intermediates (*SI Appendix*, Fig. S6; nicking was even detectable for the 9 bp truncation).

Unified Model for R-Loop Formation and Dissociation by Cascade and Cas9. Our data presented above show that for two distinct CRISPR systems, Cascade and Cas9, the PAM controls tightly the R-loop formation kinetics but leaves the R-loop stability practically unchanged. Thus, the PAM provides a kinetic rather than a thermodynamic control of R-loop formation. Distal protospacer mutations affected the R-loop stability but hardly altered the formation kinetics. This reveals for both systems a unidirectionality in the R-loop formation and dissociation cycle, which is additionally supported by the differential dependence of the first and second dissociation steps of Cascade on protospacer truncations and PAM mutations, respectively. We summarize our findings in a unified scheme for R-loop formation and dissociation by type I and II systems (Fig. 5 and *SI Appendix*, Fig. S11) that extends previous unidirectional R-loop formation models. Firstly, the RNP uses DNA distortion, guided by PAM binding, to accomplish homology search. Because R-loop formation times (down to ~1 s for Cas9) are dependent on RNP concentration, 3D diffusion must be an integral part of the target search pathway. Matching hydrogen bonding between the crRNA and the protospacer then leads to propagation of R-loop formation over the adjacent base pairs. Under unfavorable energetic conditions (high positive torque or mismatches between the protospacer and crRNA), R-loop dissociation occurs in a PAM-independent manner. While the torque that dissociates Cas9 is about half the maximum torque an RNA polymerase can generate (33), Cascade exceeds the RNA polymerase torque about twofold, representing a major difference between the two RNP classes. The high torsional stability of Cascade is not attributable to a large energetic bias (Fig. 2*C*) but rather to a ratchet-like asymmetry in the energy landscape (*SI Appendix*, *SI Theory*). This increased stability seems to be achieved by an extra "locking" step after most of the R-loop has been formed (*SI Appendix*, Fig. S11), which was revealed by the bistability of R-loops for a 4-bp truncated protospacer (Fig. 4*A*) and the two-step process for R-loop dissociation (Fig. 2*A*). We suggest that the locking is attributable to domain reorganization within Cascade, such as movement of $CasB_2$ stabilizing the free, non-target DNA strand (13). The locking step represents an additional proofreading that ensures that complementarity between the crRNA and protospacer leads to complete R-loop expansion. A similar locking was not observed for Cas9. Consequently, Cas9 can efficiently cut a protospacer with a 7-bp truncations, albeit at a reduced rate (*SI Appendix*, Fig. S6). Nonetheless, Cas9 efficiently discriminates targets over 11 bp adjacent to the PAM

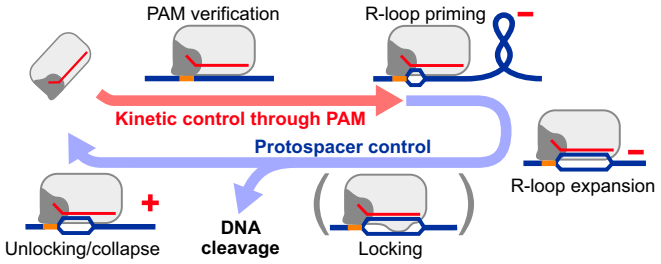

Fig. 5. Unified model for the differential control of R-loop formation and dissociation by PAM and protospacer sequences. The locking step is only observed for Cascade and not for Cas9. Red positive (+) and negative (–) symbols indicate where supercoiling of the respective sign can accelerate the step.

similarly to Cas9 from *Streptococcus pyogenes* (21). Despite complementarity, R-loops of 11 bp or shorter were not formed, revealing that Cas9 can sense further into the protospacer to identify the correct target. Structurally, this likely originates from the more extensive amino acid contacts with the heteroduplex in this particular region (34) (*SI Appendix*, *SI Theory*). Such a length threshold-dependent, all-or-none R-loop formation mechanism goes beyond a simple unidirectional model and deserves further attention. Recently, Cas9 has attracted enormous interest in genetic engineering applications (35). Based on our findings, off-target effects should mostly depend on ∼11-bp proximal to (but not distal from) the PAM.

In summary, our methodology can clearly resolve the R-loop formation processes at target DNA in real time and was used to substantiate a unidirectional R-loop formation model. Further probing of R-loop progression [e.g., through mutations in the PAM-adjacent seed sequence or through noncomplementary bubbles (21)] will help produce a high-resolution picture of target site recognition by different CRISPR-Cas systems.

Materials and Methods

DNA and Proteins. Cascade with crRNA matching spacer 1 of the *St*-CRISPR4 system and Cas9 with crRNA matching spacer 1 of the *St*-CRISPR3 system was purified and reconstituted as described in the additional methods (12, 16, 18). If not stated otherwise, DNA substrates for the Cascade experiments contained protospacer S1 and an AA PAM and for the Cas9 experiments contained protospacer S2 and a tGGtG PAM (see Fig. 1*A* and *SI Appendix*, Tables S2 and S3 for sequences), both being fully complementary to their respective crRNA.

Single-Molecule Experiments. Single-molecule assays with Cascade were performed in 20 mM Tris·HCl (pH 8.0), 150 mM NaCl, and 0.1 mg/mL BSA; assays with Cas9 were performed in 10 mM Tris·HCl (pH 7.5), 100 mM NaCl, 1 mM EDTA, 0.1 mM DTT, and 5 μg/mL BSA. Measurements were performed using 10 nM Cascade or 1 nM Cas9 unless otherwise noted. An in-house-built (26) (Cascade) or a commercial PicoTwist (Cas9) magnetic tweezers microscope was used. DNA molecules were bound to 1-μm magnetic beads (MyOne; Invitrogen) and anchored in the flow cells (36, 37). After DNA stretching and initial characterization of the DNA, proteins were added, and changes in DNA length were observed as a function of applied force and DNA turns. Torque values were calculated based on previous theoretical work (24, 38) (*SI Appendix*). In-house-written software used for these calculations is available for download at the Web site of R.S. (www.uni-muenster.de/Biologie.AllgmZoo/Gruppen/Seidel/Download).

ACKNOWLEDGMENTS. We thank S. Clausing, G. Scheidgen-Kleyboldt, and I. Kowsky for the preparation of DNA constructs. The work was supported by Biotechnology and Biological Sciences Research Council Grant BB/L000873 and Wellcome Trust Grant 084086 (to M.D.S.), European Research Council Starting Grant 261224 (to R.S.), and the European Social Fund under Global Grant Measure Grant R100 (to V.S.).

1. Garneau JE, et al. (2010) The CRISPR/Cas bacterial immune system cleaves bacteriophage and plasmid DNA. *Nature* 468(7320):67–71.
2. Hale CR, et al. (2009) RNA-guided RNA cleavage by a CRISPR RNA-Cas protein complex. *Cell* 139(5):945–956.
3. Zhang J, et al. (2012) Structure and mechanism of the CMR complex for CRISPR-mediated antiviral immunity. *Mol Cell* 45(3):303–313.
4. Brouns SJJ, et al. (2008) Small CRISPR RNAs guide antiviral defense in prokaryotes. *Science* 321(5891):960–964.
5. Carte J, Wang R, Li H, Terns RM, Terns MP (2008) Cas6 is an endoribonuclease that generates guide RNAs for invader defense in prokaryotes. *Genes Dev* 22(24):3489–3496.
6. Mojica FJM, Díez-Villaseñor C, García-Martínez J, Soria E (2005) Intervening sequences of regularly spaced prokaryotic repeats derive from foreign genetic elements. *J Mol Evol* 60(2):174–182.
7. Bolotin A, Quinquis B, Sorokin A, Ehrlich SD (2005) Clustered regularly interspaced short palindrome repeats (CRISPRs) have spacers of extrachromosomal origin. *Microbiology* 151(Pt 8):2551–2561.
8. Barrangou R, et al. (2007) CRISPR provides acquired resistance against viruses in prokaryotes. *Science* 315(5819):1709–1712.
9. Deveau H, et al. (2008) Phage response to CRISPR-encoded resistance in Streptococcus thermophilus. *J Bacteriol* 190(4):1390–1400.
10. Makarova KS, et al. (2011) Evolution and classification of the CRISPR-Cas systems. *Nat Rev Microbiol* 9(6):467–477.
11. Jore MM, et al. (2011) Structural basis for CRISPR RNA-guided DNA recognition by Cascade. *Nat Struct Mol Biol* 18(5):529–536.
12. Sinkunas T, et al. (2013) In vitro reconstitution of Cascade-mediated CRISPR immunity in Streptococcus thermophilus. *EMBO J* 32(3):385–394.
13. Wiedenheft B, et al. (2011) Structures of the RNA-guided surveillance complex from a bacterial immune system. *Nature* 477(7365):486–489.
14. Westra ER, et al. (2012) CRISPR immunity relies on the consecutive binding and degradation of negatively supercoiled invader DNA by Cascade and Cas3. *Mol Cell* 46(5):595–605.
15. Sinkunas T, et al. (2011) Cas3 is a single-stranded DNA nuclease and ATP-dependent helicase in the CRISPR/Cas immune system. *EMBO J* 30(7):1335–1342.
16. Gasiunas G, Barrangou R, Horvath P, Siksnys V (2012) Cas9-crRNA ribonucleoprotein complex mediates specific DNA cleavage for adaptive immunity in bacteria. *Proc Natl Acad Sci USA* 109(39):E2579–E2586.
17. Jinek M, et al. (2012) A programmable dual-RNA-guided DNA endonuclease in adaptive bacterial immunity. *Science* 337(6096):816–821.
18. Karvelis T, et al. (2013) crRNA and tracrRNA guide Cas9-mediated DNA interference in Streptococcus thermophilus. *RNA Biol* 10(5):841–851.
19. Semenova E, et al. (2011) Interference by clustered regularly interspaced short palindromic repeat (CRISPR) RNA is governed by a seed sequence. *Proc Natl Acad Sci USA* 108(25):10098–10103.
20. Wiedenheft B, et al. (2011) RNA-guided complex from a bacterial immune system enhances target recognition through seed sequence interactions. *Proc Natl Acad Sci USA* 108(25):10092–10097.
21. Sternberg SH, Redding S, Jinek M, Greene EC, Doudna JA (2014) DNA interrogation by the CRISPR RNA-guided endonuclease Cas9. *Nature* 507(7490):62–67.
22. Howan K, et al. (2012) Initiation of transcription-coupled repair characterized at single-molecule resolution. *Nature* 490(7420):431–434.
23. Brutzer H, Luzzietti N, Klaue D, Seidel R (2010) Energetics at the DNA supercoiling transition. *Biophys J* 98(7):1267–1276.
24. Maffeo C, et al. (2010) DNA-DNA interactions in tight supercoils are described by a small effective charge density. *Phys Rev Lett* 105(15):158101.
25. Mosconi F, Allemand JF, Bensimon D, Croquette V (2009) Measurement of the torque on a single stretched and twisted DNA using magnetic tweezers. *Phys Rev Lett* 102(7):078301.
26. Klaue D, Seidel R (2009) Torsional stiffness of single superparamagnetic microspheres in an external magnetic field. *Phys Rev Lett* 102(2):028302.
27. Kauert DJ, Kurth T, Liedl T, Seidel R (2011) Direct mechanical measurements reveal the material properties of three-dimensional DNA origami. *Nano Lett* 11(12):5558–5563.
28. Forth S, et al. (2008) Abrupt buckling transition observed during the plectoneme formation of individual DNA molecules. *Phys Rev Lett* 100(14):148301.
29. Oberstrass FC, Fernandes LE, Bryant Z (2012) Torque measurements reveal sequence-specific cooperative transitions in supercoiled DNA. *Proc Natl Acad Sci USA* 109(16):6106–6111.
30. Günther K, Mertig M, Seidel R (2010) Mechanical and structural properties of YOYO-1 complexed DNA. *Nucleic Acids Res* 38(19):6526–6532.
31. Lipfert J, Klijnhout S, Dekker NH (2010) Torsional sensing of small-molecule binding using magnetic tweezers. *Nucleic Acids Res* 38(20):7122–7132.
32. Sashital DG, Wiedenheft B, Doudna JA (2012) Mechanism of foreign DNA selection in a bacterial adaptive immune system. *Mol Cell* 46(5):606–615.
33. Ma J, Bai L, Wang MD (2013) Transcription under torsion. *Science* 340(6140):1580–1583.
34. Nishimasu H, et al. (2014) Crystal structure of Cas9 in complex with guide RNA and target DNA. *Cell* 156(5):935–949.
35. Mali P, Esvelt KM, Church GM (2013) Cas9 as a versatile tool for engineering biology. *Nat Methods* 10(10):957–963.
36. Schwarz FW, et al. (2013) The helicase-like domains of type III restriction enzymes trigger long-range diffusion along DNA. *Science* 340(6130):353–356.
37. Luzzietti N, Knappe S, Richter I, Seidel R (2012) Nicking enzyme-based internal labeling of DNA at multiple loci. *Nat Protoc* 7(4):643–653.
38. Schöpflin R, Brutzer H, Müller O, Seidel R, Wedemann G (2012) Probing the elasticity of DNA on short length scales by modeling supercoiling under tension. *Biophys J* 103(2):323–330.